^{237}U neutron-induced fission cross section

V. M. Maslov
Joint Institute of Nuclear and Energy Research - "Sosny", 220109 Minsk, Belarus
(Received 8 July 2005; published 31 October 2005)

The neutron-induced fission cross section of ^{237}U target nuclide is calculated consistently with the ^{238}U(n,F), ^{238}U(n, $2n$) and ^{238}U(n, $3n$) reaction cross section up to $E_n \sim 20$ MeV. The fission probability of the ^{238}U nuclide, fissioning in ^{238}U(n, nf) reaction is shown to be compatible with the surrogate ^{236}U(t, pf) fission probability and ratio of fission probability $P_f(^{238}\mathrm{U}(d, d'f))/P_f(^{236}\mathrm{U}(d, d'f))$, data up to $E_n \sim 14$ MeV. The ^{238}U(n, nf) reaction contribution to the observed ^{238}U(n,F) cross section up to $E_n \sim 9$ MeV is defined by the collective levels of the ^{238}U at saddle deformations, lying within the pairing gap. The importance of the lowering of anomalous rotational γ-band $K^\pi = 2^+$ band levels at saddle deformations is demonstrated. The excitation of the two-quasiparticle states at saddle deformations of the fissioniong ^{238}U nuclide is evidenced.^{237}U fission cross section is predicted up to $E_n \sim 200$ MeV.

DOI: 10.1103/PhysRevC.72.044607 PACS number(s): 25.85.−w, 27.90.+b

I. INTRODUCTION

Uranium-237 has rather short half-life of 6.75 d, which almost prohibited the differential measurements of neutron-induced fission cross section. The only measurement of that kind is the time-of-flight measurement with the underground bomb-shot by McNally *et al.* [1]. It is supplemented with the integral measurements in critical assemblies or reactor, however, these measurements turned out to be in serious conflict with the later differential measurement by McNally *et al.* [1] (see Ref. [2] and references therein). The fission cross section estimate by Cramer and Britt [3], which was based on fission probability estimate of ^{238}U, excited in the reaction ^{236}U(t, pf), supported the cross section data by McNally *et al.* [1] at $E_n \sim 0.15$ MeV. Recently a number of theoretical evaluations of ^{237}U(n, f) cross sections appeared, which differed from each other and older evaluations very much [2,4–8] in the energy range of $0.1 \sim 20$ MeV. Fortunately, extensive surrogate ^{236}U(t, pf) fission probability data have appeared, from which the ^{237}U(n, f) cross section was estimated for the incident neutron energies from $E_n \sim 0.15$ MeV up to $E_n \sim 2.5$ MeV [9]. The main difficulty of such estimation is the correct modelling of the spin population differences in transfer, i.e., (t, pf), and neutron-induced reactions [10], it seems the problem was almost solved by consistent analysis of ^{234}U(t, pf) and ^{235}U(n, f) data. However, more advantageous is the approach introduced recently by Plettner *et al.* [11], which measures the ratio of fission probabilities of ^{238}U and ^{236}U nuclides. This ratio was measured for the deuteron-induced fission events, i.e., the ratio of $P_f(^{236}\mathrm{U}(d, d'f))/P_f^{238}(\mathrm{U}(d, d'f))$. The ratio data by Plettner *et al.* [11] allow us to construct a neutron-induced fission cross section of ^{237}U target nuclide for the incident energy range of $E_n \sim 0.1$–14 MeV.

Alternatively, the fission probability of the ^{238}U nuclide could be fixed by the ^{238}U(n,F) observed neutron-induced fission cross section description above the ^{238}U(n, nf) emissive fission threshold. In the interaction of neutrons with the U nuclei at incident neutron energies $E_n \gtrsim 6$ MeV, x prefission (or presaddle) neutrons might be emitted, before the fissioning nuclide reaches the outer saddle point. This peculiarity leads to the multiple-chance fission contributions to the observed fission cross section ^{238}U(n,F). A number of fissioning nuclides might contribute to the fission observables, it amounts to $\sim$3 for the ^{238}U(n, xnf) fission reaction at $E_n \sim 20$ MeV. Relative contributions of multichance (emissive) ^{238}U(n, xnf) and first-chance (nonemissive) ^{238}U(n, f) fission reactions to the observed fission cross section of ^{238}U(n,F) much depend upon the ^{239}U nuclide fissility, as well as fissilities of $^{239-x}$U nuclei. The second-chance fission ^{238}U(n, nf) contribution remains systematically lower than that of the first-chance fission reaction ^{238}U(n, f), however, well above the ^{238}U(n, nf) reaction threshold, almost one-half of the observed fission cross section comes from the fission of the ^{238}U nuclide [12,13]. For partitioning of the observed fission cross section (n,F) into emissive (n, xnf) and nonemissive (n, f) fission contributions the theoretical estimate of the ^{238}U(n, f) first-chance fission reaction cross section is of crucial importance. First-chance fission cross section shape for $^{232–238}$U target nuclides for incident neutron energies above emissive fission threshold and up to $\sim$20 MeV is a complex function of the fission probability of composite n+U equilibrated nuclide, neutron reaction cross section $\sigma_r(E_n)$ and a fraction of the preequilibrium emission of the first neutron $q(E_n)$. It cannot be viewed as a pure continuation of the first-chance fission cross section shape from the first "plateau" region to the higher incident neutron energies. Fortunately, the uncertainty of the theoretical definition of the multichance fission structure is sufficiently reduced by the consistent description of the ^{238}U(n,F), ^{238}U(n, $2n$), and ^{238}U(n, $3n$) reaction cross sections up to $E_n \sim 20$ MeV. A similar approach was previously used for the description of the fission and (n, $2n$) reaction cross sections for the ^{232}Th target nuclide [14] and fission, (n, $2n$) and (n, $3n$) reaction cross sections for the ^{235}U target nuclide [15].

Valuable information, justifying the calculated multichance fission contributions to the fission observables could be obtained by the analysis of prompt fission neutron spectra (PFNS). Emission of one or two neutrons in (n, nf) or (n, $2nf$) reactions strongly influences the observed prompt

fission neutron spectra shape, as it was demonstrated for the neutron-induced fission of ^{238}U(n,F) and ^{232}Th(n,F) [12,13] and then for ^{235}U(n,F) [15] reaction. Exclusive (n, xnf) prefission neutron spectra were calculated simultaneously with fission and (n, xn) reaction cross sections. PFNS shapes for the ^{238}U(n,F) and ^{232}Th(n,F) observed fission reactions were described [12,13] for the incident neutron energy ranges $E_n \sim$ 7–17.7 MeV and $E_n \sim$ 14.7–17.7 MeV, respectively. High energy tails of first neutrons of (n, nf) and $(n, 2nf)$ reactions are shown to be evidenced in PFNS measured data trends for ^{238}U(n,F) and ^{232}Th(n,F) PFNS. Similar analysis based on the calculated exclusive (n, xnf) prefission neutron spectra, was accomplished in case of ^{235}U(n,F) reaction in the emissive fission domain [15]. Actually, the energy dependence of PFNS of ^{238}U(n,F) reaction for prompt fission neutron energies $\varepsilon \lesssim E_{\rm th} \sim E_n - B_f$ resembles the shape of the fission probability P_f of ^{238}U residual nuclide, B_f being effective fission barrier value of ^{238}U. The energy dependences of PFNS for other target nuclides, i.e., ^{235}U and ^{232}Th for $\varepsilon \lesssim E_{\rm th}$ resemble the shapes of the fission probabilities P_f of ^{235}U or ^{232}Th nuclides, respectively. The ^{231}Th target nuclide as well as ^{237}U are rather short-lived, their neutron-induced fission cross sections are poorly investigated experimentally, however, it was shown [14] that the ^{230}Th(t, pf) surrogate fission data [9,10] for $E_n \sim$ 0.1–1.9 MeV are quite compatible with the present model estimate. The strong point of ^{235}U(n,F) multichance fission partitioning is that fission probabilities of the residual nuclides ^{235}U and ^{234}U are well investigated experimentally via ^{234}U(n, f) and ^{233}U(n, f) reactions, respectively. The detailed analysis of the neutron cross sections of ^{234}U [16] and ^{233}U [17] target nuclides, as well as numerical data on neutron cross sections are available at the web server of the Nuclear Data Section of International Atomic Energy Agency: http://www-nds.iaea.org/minskact/ [16,17]. The measured fission cross section of ^{235}U(n,F) is described with Hauser-Feshbach approach consistently with the ^{235}U$(n, 2n)$ and ^{235}U$(n, 3n)$ reaction cross sections. Any variation of the contributions of ^{235}U(n, nf) or ^{235}U$(n, 2nf)$ reactions to the ^{235}U observed fission cross section would either deteriorate ^{235}U$(n, 2n)$ and ^{235}U$(n, 3n)$ reaction cross section description or description of the measured ^{234}U(n, f) [16] and ^{233}U(n, f) [17] fission cross sections, or both. A similar conclusion is valid also in the case of ^{238}U+n interaction data [13] and ^{232}Th+n interaction data [14].

Once again, first-chance fission cross section for incident neutron energies up to 20 MeV, extracted by consistent description of the three data sets: ^{238}U(n,F), ^{238}U$(n, 2n)$, ^{238}U$(n, 3n)$; ^{232}Th(n,F), ^{232}Th$(n, 2n)$; ^{235}U(n,F), ^{235}U$(n, 2n)$, ^{235}U$(n, 3n)$ could be viewed as model-independent estimates. That would define positively the reliability of the first-chance fission cross section estimate of the ^{237}U(n, f) reaction for incident neutron energies up to (n, nf) emissive fission threshold. At higher incident energies, when fissioning ^{237}U and ^{236}U nuclides contribute to the observed ^{237}U(n,F) fission cross section via ^{237}U(n, nf) and ^{237}U$(n, 2nf)$, respectively, the reliability of present estimate of the observed ^{237}U(n,F) cross section is supported by the ^{236}U(n, f) and ^{235}U(n, f) cross section description and overall systematics of fission cross sections of N-odd target nuclides, i.e., ^{233}U(n,F), ^{235}U(n,F) and ^{237}U(n,F). The consistency of the extracted fission probability of the ^{238}U nuclide, fissioning in the ^{238}U(n, nf) reaction and calculated ^{237}U(n,F) fission cross section with the surrogate ^{236}U(t, pf) [9] and ^{236}U$(d, d'f)$ fission probability data [11] will be demonstrated.

II. STATISTICAL MODEL

The ^{237}U and ^{238}U neutron-induced fission cross section are calculated within the Hauser-Feshbach theory for $E_n \sim$ 0.001–20 MeV, the coupled channel optical model and the double-humped fission barrier model are used. Level densities of fissioning and residual nuclei as well as fission barrier parameters are key ingredients, involved in neutron-induced fission cross section calculations. Fission of ^{238}U nuclide, either in ^{238}U(n, nf) or ^{237}U(n, f) reactions, is of main interest. The fissioning nuclide ^{238}U is even-even, that means for intrinsic excitations below the pairing gap its fission probability would be defined by the collective levels of ^{238}U at saddle deformations. At excitations above a pair breaking threshold, when excitation of the two-quasiparticle, four-quasiparticle, etc., states is possible, the fission probability of the ^{238}U would be defined by the relevant level densities. Some guidance regarding the collective bands structure at saddle deformations could be obtained from the description of the neutron-induced fission cross sections of ^{233}U and ^{235}U target nuclides in the incident neutron energy range of $E_n \sim$ 0.001–2 MeV. The description of the ^{238}U(n,F) cross section above emissive fission threshold will be used to fix the structure of the collective levels and the level density of the ^{238}U nuclide at saddle deformations. Below is the outline of the statistical model [18–21] employed.

A. Fission cross section

Above the emissive fission threshold contributions of emissive fission to the observed fission cross section, coming from the (n, xnf), $x = 1, \ldots X$, multichance fission reactions of relevant equilibrated uranium nuclei, could be calculated as

$$\sigma_{nF}(E_n) = \sigma_{nf}(E_n) + \sum_{x=1}^{X} \sigma_{n,xnf}(E_n), \qquad (1)$$

multichance fission contributions are calculated using the fission probability estimates $P_{fi}^{J\pi}(U)$ as

$$\sigma_{n,xnf}(E_n) = \sum_{J\pi} \int_0^{U_{\rm max}^{x+1}} W_{x+1}^{J\pi}(U) P_{f(x+1)}^{J\pi}(U) dU, \qquad (2)$$

where $W_x^{J\pi}(U)$ is the population of the $(x+1)-$th nucleus at excitation energy U after emission of x neutrons. The excitation energy $U_{\rm max}^{x+1}$ depends on the incident neutron energy E_n and the energy, removed from the composite $n+^{238(237)}$U system by the prefission neutrons of the $^{238(237)}$U(n, xnf) reaction. The fission probabilities $P_{fx}^{J\pi}$ of the fissioning nuclides ^{238}U, ^{237}U, and ^{236}U define the emissive fission contributions of ^{238}U(n, nf), ^{238}U$(n, 2nf)$ and ^{238}U$(n, 3nf)$, respectively. For

^{237}U target there is a shift of mass numbers by one mass unit. The emissive fission contributions depend on the fission barrier and level density parameters of the fissioning and residual U nuclei.

The behavior of the first-chance fission cross section $\sigma_{nf}(E_n)$ above the emissive fission threshold is obviously related to the energy dependence of the fission probability of the composite n+U nuclide $P_f^{J\pi}(E_n)$ for the compound nucleus state J^π [22]:

$$\sigma_{nf}(E_n) = (1 - q(E_n))\frac{\pi\lambda^{2}}{2(2I+1)} \times \sum_{lJ\pi}(2J+1)T_l(E_n)P_f^{J\pi}(E_n), \quad (3)$$

I and l being target nucleus spin and neutron angular momentum, respectively. The contribution of the first neutron preequilibrium emission $q(E_n)$ to the neutron emission spectrum is fixed by the description of the high-energy tail of the ^{238}U$(n, 2n)$ reaction [23]. First-chance fission cross section $\sigma_{nf}(E_n)$ is defined by the first-chance fission probability of the composite n+U equilibrated nuclide.

For incident neutron energies lower than the emissive fission threshold, the first-chance fission cross section $\sigma_{nf}(E_n)$ is defined in a Hauser-Feshbach-Moldauer [24] formalism, using width fluctuation correction and taking into account channel spin $\vec{j} = \vec{I} + \vec{\frac{1}{2}}$, ($\vec{J} = \vec{l} + \vec{j}$) dependence of the neutron transmission coefficients as

$$\sigma_{nf}(E_n) = (1 - q(E_n))\frac{\pi\lambda^{2}}{2(2I+1)} \times \sum_{ljJ\pi}(2J+1)T_{lj}^{J\pi}(E_n)P_f^{J\pi}(E_n)S_{nf}^{ljJ\pi}, \quad (4)$$

the compound nucleus fission probability $P_f^{J\pi}$ for the compound state J^π is

$$P_f^{J\pi}(E_n) = \frac{T_f^{J\pi}(U)}{T_f^{J\pi}(U) + T_n^{J\pi}(U) + T_\gamma^{J\pi}(U)}, \quad (5)$$

where $U = B_n + E_n$ is the excitation energy of the compound nucleus n+U, B_n is the neutron binding energy, $T_{lj}^{J\pi}(T_l)$ are the entrance neutron transmission coefficients for the channel $(ljJ\pi)(l)$. The fission probability $P_f^{J\pi}(E_n)$ of the compound nucleus with excitation energy U for the given spin J and parity π, depends on the $T_f^{J\pi}$, $T_n^{J\pi}(U)$, and $T_\gamma^{J\pi}(U)$ transmission coefficients of the fission, neutron scattering, and radiative decay channels, $S_{nf}^{ljJ\pi}$ denotes the partial widths Porter-Thomas fluctuation factor. The procedure for calculation of the transmission coefficient for the radiative decay channel is described elsewhere [25]. For the calculation of corrections due to width fluctuations only Porter-Thomas fluctuations are taken into account. The effective number of the degrees of freedom for the fission channel is defined at the higher fission barrier saddle as $\nu_f^{J\pi} = T_f^{J\pi}/T_{f\max}^{J\pi}$, where $T_{f\max}^{J\pi}$ is the maximum value of the fission transmission coefficient $T_f^{J\pi}$. At incident neutron energies higher than the cut-off energy U_c of the discrete level spectrum of the target nuclide, the approach by Tepel *et al*. [26] is employed, it approximates the cross section behavior in case of a large number of open exit channels.

A coupled channel model is employed to estimate the entrance neutron transmission coefficients $T_{lj}^{J\pi}$(or T_l). We adopted here the optical potential parameters obtained for n+^{238}U interaction by fitting total cross section data, angular distributions, and s-wave strength function [27]. The direct excitation of the ground state rotational band levels of ^{238}U, $0^+-2^+-4^+-6^+-8^+$, is estimated within the rigid rotator model, five levels of the ground state band are assumed coupled. For the ^{237}U target nuclide we adopted the optical potential parameters obtained for the ^{235}U [15], the direct excitation contributions for the ground state rotational band levels of ^{237}U target, $1/2^+-3/2^+-5/2^+-7/2^+-9/2^+-11/2^+$, are estimated within the rigid rotator model, six levels of the ground state band are assumed coupled.

B. Fission channel

Fission probabilities $P_{fx}^{J\pi}$ of the fissioning nuclides $^{239(238)}$U, $^{238(237)}$U, and $^{237(236)}$U define the first-chance and emissive fission contributions of $^{238(237)}$U(n, f), $^{238(237)}$U(n, nf), and $^{238(237)}$U$(n, 2nf)$, respectively. They depend on the fission barrier and level density parameters of fissioning and residual U nuclei. Inner and outer fission barrier heights and curvatures as well as parameters of the level densities at both saddles are the model parameters. Fission barrier height values and saddle symmetries are strongly interdependent. The order of symmetry of nuclear shape at saddles, which influences both level density and fission barrier, was defined by Howard and Möller [28] within shell correction method (SCM) calculation. We adopt the saddle point asymmetries from these [28] SCM calculations. They predict also $E_{fA} < E_{f\mathrm{BAS}}$ in the mass range $A < 253$, $E_{f\mathrm{BAS}}$ being the outer barrier height for the mass-asymmetric fission. According to the SCM calculations of Howard and Möller [28] the inner barrier of U nuclei with $A \leqslant 236$ was assumed axially symmetric, as well as nuclear shape at ground state deformations. This peculiarity helped to interpret also the nonthreshold fission cross section behavior of ^{232}U(n, f) [29] assuming a lowered height of axially symmetric inner hump of ^{233}U, as anticipated by Howard and Möller [28] with SCM calculations. Inner saddle shapes of U nuclei with $A > 236$ are assumed triaxial. Outer barrier for asymmetric fission of uranium nuclei is assumed to be mass-asymmetric. In principle, the fission barrier of light U ($A = 234$, 236) nuclei might be rather complex, it might be three-humped, as it was predicted by Howard and Moller [28]. Analysis of the fission probability of ^{236}U in ^{235}U(d, pf) reaction by Ref. [30] enabled the determination of the $E_A = 5.05 \pm 0.20$ MeV, it was estimated to be $\sim$1 MeV lower than the outer barrier B, which may be splitted and have one more (third) rather deep well. Fortunately, the influence of the outer barrier $B(E_B = 6.1$ MeV) splitting of the ^{236}U nuclide on the observed neutron-induced ^{235}U(n, f) [and ^{237}U$(n, 2nf)$] fission cross section would not be much important for the excitation energies of actual interest. This allows us to simplify the calculation of the fission probability of ^{236}U, which

contributes to the ^{237}U(n,F) cross section via ^{237}U$(n, 2nf)$ reaction, i.e., we will approximate the fission barrier of ^{236}U nuclei with a double-humped barrier, i.e., ignore the splitting of the outer barrier B. For $A > 236$, like in the case of ^{238}U nuclide, fissioning in ^{237}U(n, f) or ^{238}U(n, nf) reaction, $E_{fA} > E_{f\mathrm{BAS}}$ is assumed (more detailed discussion about theoretical and experimental fission barriers of U is given below).

Neutron-induced fission in a double humped fission barrier model [31] could be considered in a complete damping approximation, i.e., it could be viewed as a two-step process, i.e., a successive crossing over the inner hump A and over the outer hump B. Hence, the transmission coefficient of the fission channel $T_f^{J\pi}(U)$ can be represented as

$$T_f^{J\pi}(U) = \frac{T_{fA}^{J\pi}(U) T_{fB}^{J\pi}(U)}{\left(T_{fA}^{J\pi}(U) + T_{fB}^{J\pi}(U)\right)}. \quad (6)$$

The transmission coefficient $T_{fi}^{J\pi}(U)$ is defined by the level density $\rho_{fi}(\varepsilon, J, \pi)$ of the fissioning nucleus at the inner and outer barrier humps ($i = A, B$, respectively):

$$T_{fi}^{J\pi}(U) = \sum_{K=-J}^{J} T_{fi}^{JK\pi}(U) + \int_0^U \frac{\rho_{fi}(\varepsilon, J, \pi) d\varepsilon}{(1 + \exp(2\pi(E_{fi} + \varepsilon - U)/\hbar\omega_i))}, \quad (7)$$

where the first term denotes the contributions $T_{fi}^{JK\pi}(U)$ of the low-lying collective states (JK^π) and the second term—that from the continuum levels at the saddle deformations, $\varepsilon = U - E_{fi}$ is the intrinsic excitation energy of the fissioning nucleus, E_{fi} and $\hbar\omega_i$ are the height and curvature of the i+th fission barrier hump, respectively. The first term contribution due to the discrete transition states depends upon the fission saddle symmetry, they would be modelled for the ^{238}U nuclide, a starting collective level bands are those used for transition states modelling of ^{236}U, ^{234}U, or ^{232} Th [14]. The level density $\rho_{fi}(\varepsilon, J, \pi)$ of the fissioning nucleus is also determined by the order of symmetry of nuclear saddle deformation.

1. Fission transmission coefficient

The contribution of the second-chance fission ^{238}U(n, nf) to the observed fission cross section of ^{238}U(n,F) (see Fig. 1) for the incident neutron energies $E_n = 6 \sim 9$ MeV, is defined mainly by the ^{238}U collective states lying within the pairing gap. Each collective state in the even fissioning nuclide ^{238}U is assumed to have a rotational band built on it with a rotational constant $F_0/\hbar^2$, dependent upon the respective saddle deformation. Inner saddle is assumed to be axially asymmetric, while outer saddle axially symmetric but mass asymmetric. The latter peculiarity would lead to the lowering of the negative parity octupole vibration bands at deformations of the outer saddle B. Triaxiality at inner saddle would be pronounced in lowering of the anomalous rotational γ-band $K^\pi = 2^+$ levels [32]. At higher incident neutron energies $E_n \gtrsim 9$ MeV, the intrinsic excitation energy of the fissioning ^{238}U nuclide might be higher than the threshold energy U_2,

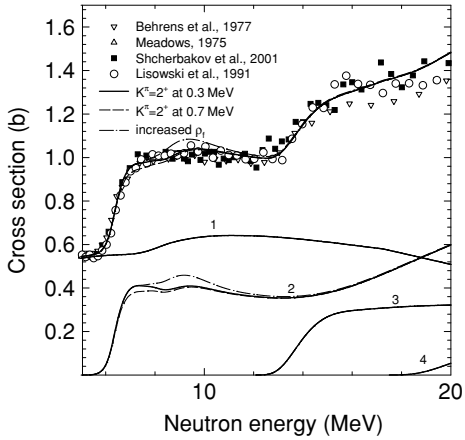

FIG. 1. ^{238}U(n,F) cross section. The solid line shows a fit to the observed fission cross section, $\delta_{2f} = 0.85$ MeV; the dot-dashed line shows the sensitivity of the calculated fission cross section to the increased two-quasiparticle state density of ^{238}U at saddle deformations, $\delta_{2f} = 0.65$ MeV; dashed and solid curves show the sensitivity of the calculated fission cross section to the lowering of anomalous γ-band $K^\pi = 2^+$ of ^{238}U at outer saddle deformations due to axial asymmetric deformations; Labels "1," "2," "3," and "4" denote first-, second-, third-, and fourth-chance fission cross sections.

corresponding to the excitation of the two-quasiparticle states at higher (inner) saddle deformations of the ^{238}U nuclide.

The collective levels of ^{238}U [33] at ground state deformations, lying within the pairing gap, were interpreted within a soft rotator model [34–37]. The structures of the quadrupole transversal γ-vibration $K^\pi = 0_2^+$, anomalous rotational γ-vibration $K^\pi = 2_1^+$, quadrupole longitudinal β-vibration $K^\pi = 0_3^+$ bands as well as first octupole $K^\pi = 0_1^-$ band levels were analyzed with the deformed nonaxial, soft to quadrupole β- and γ-vibrations rotator [34–37]. The excitation energies of the members of the even-parity collective bands $K^\pi = 0_1^+, 0_2^+, 0_3^+, 2_1^+$ and the first octupole band $K^\pi = 0_1^-$, were reproduced up to ~2 MeV excitations.

The levels of the $K^\pi = 0_1^-$ band (0.6801 MeV) are most sensitive to the octupole deformation parameter β_3, which slightly influence also the positions of other collective band levels. Another parameter which defines the positions of levels of the $K^\pi = 0_1^-$ band is the softness parameter to the octupole vibrations μ_ξ, this peculiarity prohibits an unanimous definition of the β_3-parameter by fitting the $K^\pi = 0_1^-$ band levels' positions only. When this coupling strength parameter β_3 is changed to fit the angular distribution data, the level positions could be kept unaffected with this softness parameter μ_ξ. This procedure was followed in the case of ^{238}U inelastic scattering data analysis [38]. Data for a group of octupole band levels by Plompen *et al.* [39] up to $E_n \sim 3$ MeV helped to define uniquely the β_3-parameter and softness parameter to the octupole vibrations μ_ξ. The levels of the second $K^\pi = 0_2^+$ band (0.9257 MeV) are classified as quadrupole transversal γ-vibrations, they are defined by the softness parameter to respective vibrations μ_γ. Anomalous rotational γ-band $K^\pi = 2^+$ levels are defined by the nonaxiality parameter γ_o, which is correlated with the position of $K^\pi \simeq 2^+$ level. The $K^\pi = 0_3^+$ band (0.993 MeV)—that of

TABLE I. Transition spectra band-heads of ^{238}U nuclide.

Inner saddle		Outer saddle		Ground state deformation	
K^π	E_{K^π}, MeV	K^π	E_{K^π}, MeV	K^π	E_{K^π}, MeV
0_1^+	0.0	0_1^+	0.0	0_1^+	0.0; $J^\pi = 0^+,2^+,4^+,6^+\ldots$
0_2^+		0_2^+		0_2^+	0.9257 (γ-vib.); $J^\pi = 0^+,2^+,4^+,6^+\ldots$
2_1^+	0.1	2_1^+	0.7	2_1^+	1.0603 (γ-vib.);$J^\pi = 2^+,3^+,4^+,5^+,6^+\ldots$
0_1^-	0.4	0_1^-	0.05	0_1^-	0.6801 (oct-vib.); $J^\pi = 1^-,3^-,5^-\ldots$
1_1^-	0.4	1_1^-	0.05	1_1^-	0.9308 (oct-vib.); $J^\pi = 1^-,2^-,3^-,4^-\ldots$
0_3^+		0_3^+		0_3^+	0.993(β-vib.);$J^\pi = 0^+,2^+,4^+,6^+\ldots$
2_1^-	0.6	2_1^-	0.1	2_1^-	1.1287(oct-vib.); $J^\pi = 2^-,3^-,4^-,5^-\ldots$
1^+	0.75	1^+	0.75	1^+	$J^\pi = 1^+, 2^+,3^+ ,4^+,5^+,6^+$

longitudinal quadrupole β-vibrations. As regards quadrupole transversal γ-vibrations, the static nonaxiality parameter γ_o for ^{238}U was fitted to the position of the anomalous γ-band $K^\pi = 2^+$. With the increase of the quadrupole deformations, corresponding to stretching of the fissioning nucleus, the relative positions of the collective band structure of ^{238}U may change, just as they change for neighbor ^{232,234,236}U of ^{232}Th nuclides [36]. To accomplish a similar analysis of the collective band structures at saddle deformations in a soft rotator model is hardly possible, since there is almost no relevant data to fix the softness parameters μ_γ, μ_β, and μ_ξ. The investigations of the fission angular correlations in (d, pf), (t, pf) and (γ, f) reactions, referred to by Younes and Britt [10], could provide only "the lowest vibrational band with each K, and they give only approximate locations of these bands." We will assume that the structure of the positive parity collective levels at saddle deformations is generally similar to that at ground state deformations, actual relative positions would be slightly varied. The inclusion of $K^\pi = 0_2^+$ and $K^\pi = 0_3^+$ into the transition states scheme may seem questionable [40], however, without these states it is impossible to reproduce the data trends of ^{235}U(n, f) and ^{233}U(n, f) for incident neutron energies below ~1 MeV [17]. In the case of ^{237}U(n, f) reaction, since the $E_{fA} \sim B_n$, the calculated cross section is almost insensitive to the inclusion of $K^\pi = 0_2^+$ and $K^\pi = 0_3^+$ collective bands The positions of the negative parity bands, as is well known, may be lowered due to the mass asymmetric deformations. The positions of the anomalous γ-band $K^\pi = 2^+$ also may be lowered due to softness to triaxial deformations [32]. Except for the $K^\pi = 0_1^+$, $K^\pi \simeq 2_1^+$, and $K^\pi = 0_1^-$ bands, identified in the ^{238}U scheme at ground state deformations with the soft rotator model (excitation energies are given in the sixth column of Table I), three extra bands $K^\pi = 1_1^+, 1_1^-$, and 2_1^- are added. The $K^\pi = 1_1^+$ collective band levels are "excited" by the s-wave neutrons [40], however, fission via $K^\pi = 1_1^+$ transition states would not have large contribution to the observed fission cross section. At inner saddle the fission via $K^\pi = 1_1^+$ collective band transition states would be sub-barrier. We construct the discrete transition spectra of ^{238}U up to ~1.3 MeV, using the collective band heads $K^\pi = 0_1^+$, $K^\pi \simeq 2_1^+$, $K^\pi = 0_1^-$, $K^\pi = 1_1^+$, $K^\pi = 1_1^-$, and $K^\pi = 2_1^-$, shown in Table I. In the sixth column of Table I sequences of spins of the collective bands are shown. With transition state spectra thus defined, the fission barrier parameters of ^{238}U are obtained by fitting the ^{238}U(n,F) fission cross section.

C. Neutron channel

The lumped transmission coefficient of the neutron scattering channel [see Eq. (5)] is given by the equation

$$T_n^{J\pi}(U) = \sum_{l'j'q} T_{l'j'}^{J\pi}(E_n - E_q) + \sum_{l'j'I'} \int_0^{U-U_c} T_{l'j'}^{J\pi}(E_n')\rho(U - E_n', I', \pi)dE_n', \tag{8}$$

where $\rho(U - E_n', I', \pi)$ is the level density of the residual nucleus, E_q are the energies of the discrete levels of the residual nucleus. Discrete levels of the residual nuclide ^{237}U [33] are used up to ~0.63 MeV. The entrance channel neutron transmission coefficients $T_{lj}^{J\pi}$ are calculated within a rigid rotator coupled channel approach. The cross sections of the direct excitation of ground state band levels were subtracted from the absorption cross section to get the compound nucleus formation cross section.

D. Level density

The level densities of the fissioning and residual nuclei define the transmission coefficients of fission and neutron decay channels, respectively. We will briefly discuss here the level densities of even and even-odd nuclei. The level densities were calculated with a phenomenological model by Ignatyuk *et al.* [41], which takes into account shell, pairing, and collective effects in a consistent way

$$\rho(U, J, \pi) = K_{\rm rot}(U, J)K_{\rm vib}(U)\rho_{qp}(U, J, \pi), \tag{9}$$

where the quasiparticle level density $\rho_{qp}(U, J, \pi)$ is defined as

$$\rho_{qp}(U, J, \pi) = \frac{(2J + 1)\omega_{qp}(U)}{4\sqrt{2\pi}\sigma_\perp^2\sigma_\parallel} \exp\left(-\frac{J(J + 1)}{2\sigma_\perp^2}\right), \tag{10}$$

$\omega_{qp}(U)$ is the quasiparticle state density, $K_{\rm rot}(U, J)$ and $K_{\rm vib}(U)$ (for details about calculation of $K_{\rm vib}(U)$ see Ref. [41]) are factors of the rotational and vibrational enhancement of the level density. The collective contribution to the level density of deformed nuclei is defined by the nuclear deformation order of symmetry. The order of symmetry of the U nuclei shape at inner and outer saddles were adopted from the SCM calculations by Howard and Möller [28]. Since uranium nuclei with $A \leqslant 236$ are axially symmetric at both saddles [28] the

$$K_{\rm rot}(U) = \sigma_{\perp}^2 = F_{\perp} t, \tag{11}$$

where $\sigma_{\perp}^2$ is the spin cutoff parameter, $F_{\perp}$ is the nuclear momentum of inertia (perpendicular to the nucleus symmetry axis). Uranium nuclei with $A > 236$ are assumed to be axially asymmetric at inner saddle, then

$$K_{\rm rot}(U) \simeq 2\sqrt{2\pi}\sigma_{\perp}^2\sigma_{\parallel}. \tag{12}$$

The nuclear momentum of inertia $F_{\perp}$ equals the rigid-body value at high excitation energies ($U \sim 5$ MeV), where the pairing correlations are destroyed, or experimental value at "zero" temperature. For intermediate excitation energies it is interpolated using the superfluid model [41]. Another spin cutoff parameter is $\sigma_{\parallel}^2 = F_{\parallel} t = 6/\pi^2 \langle \widetilde{m}^2 \rangle a(1 - 2/3\varepsilon)t$, where $\langle \widetilde{m}^2 \rangle \simeq 0, 24A^{2/3}$ is the average value of the squared projection of the angular momentum of the single-particle states, a is the main level density parameter and ε is the quadrupole deformation parameter. The closed-form expressions for thermodynamic temperature and other relevant equations, which one needs to calculate $\rho(U, J, \pi)$, are provided by the model of Ignatyuk *et al*. [41].

To calculate the level density at the low excitation energy, i.e., just above the last discrete level excitation energy, when $N^{\rm exp}(U) \sim N(U)$, a Gilbert-Cameron-type [constant temperature model (CTM)] approach could be used, since the model by Ignatyuk *et al*. [41] underestimates the $N^{\rm exp}(U)$ at $U \lesssim 1$ MeV (for even-odd nuclei) or $U \lesssim 2$ MeV (for even-even nuclei) [42]. The constant temperature approximation of the total level density

$$\rho(U) = dN(U)/dU = T^{-1} \exp((U - U_o)/T) \tag{13}$$

is extrapolated up to the matching point U_c to the $\rho(U)$ value, calculated with a phenomenological model by Ignatyuk *et al*. [41]. This approximation of the number of low-lying levels shows that in case of ^{237}U missing of the discrete levels above $\sim$0.63 MeV is markedly pronounced, while in case of ^{238}U missing is noticed above $\sim$1.2 MeV [43]. The energy shift U_o has the meaning of the odd-even energy shift. The value of the nuclear temperature parameter T is obtained by the matching conditions at the excitation energy U_c. The matching condition is as follows:

$$U_c = U_o - T \ln(T\rho(U_c)). \tag{14}$$

This rather crude approximation of the total level density $\rho(U)$ allows us to reproduce the general trends of the observed cross sections of neutron-induced reactions. However, there are a number of signatures in the observed neutron cross sections, which might be attributed to the influence of a few-quasiparticle configurations on the state density $\omega_{qp}(U)$ and eventually on the total level density $\rho(U)$. At low intrinsic excitation energies ($U \lesssim 3$ MeV) either for even and odd U nuclei at equilibrium or saddle deformations, few-quasiparticle effects which are due to pairing correlations, are essential for the state density $\omega_{qp}(U)$ calculation [44]. Unfortunately, there is still no microscopic treatment of the influence of the pairing correlations and few-quasiparticle excitations on the level density for the realistic single-particle spectra of deformed nuclei, which reproduces measured data on the level densities without further renormalizations (see Ref. [45] and references therein). The partial m-quasiparticle state densities for even or odd U nuclides, which sum up to the intrinsic state density of quasiparticle excitations, could be modelled using the Bose-gas model prescriptions [46,47]. The intrinsic state density of quasiparticle excitations $\omega_{qp}(U)$ could be represented as a sum of m-quasiparticle state densities $\omega_{mqp}(U)$:

$$\omega_{qp}(U) = \sum_m \omega_{mqp}(U) = \sum_m \frac{g^m (U - U_m)^{m-1}}{((m/2)!)^2 (m-1)!}, \tag{15}$$

where $g = 6a/\pi^2$ is a single-particle state density at the Fermi surface, m is the number of quasiparticles. The important model parameters are the threshold values U_m for the excitation of m-quasiparticle configurations $m = 2, 4 \ldots$ for even-A nuclei or $m = 1, 3 \ldots$ for odd-A nuclei [46], they take into account the dependence of the correlation functions Δ for the $m-$quasiparticle configurations on the number of excited quasiparticles. The detailed treatment of this approach and approximations employed, as applied for fission, inelastic scattering, or capture reaction calculations, is provided in Refs. [25,42,48]. However, for the fission cross section calculations a flexible semiempirical model of the intrinsic state density $\omega_{qp}(U)$ could be used, which we would call a "modified constant temperature model (CTM)." In this approach the modelling of the total level density

$$\rho(U) = K_{\rm rot}(U) K_{\rm vib}(U) \frac{\omega_{qp}(U)}{\sqrt{2\pi}\sigma_{\parallel}} = T^{-1} \exp((U - U_o)/T) \tag{16}$$

looks like a simple renormalization of the quasiparticle state density $\omega_{qp}(U)$ at excitation energies $U < U_c$, while $U_o \simeq -k\Delta_o$, Δ_o is the pairing correlation function, $\Delta_o = 12/\sqrt{A}$, A is the mass number, $k = 2$ for the odd-odd and $k = 1$ for odd-even nuclei. The total level densities for saddle $\rho_f(U)$ or ground state $\rho_n(U)$ deformations could be modelled for the excitation energies below the four-quasiparticle states excitation threshold U_4 (even nuclei) as

$$\rho_{f(n)}(U) \cong T_{f(n)}^{-1} \exp[U_4 - U_{f(o)} - \delta_{2f(n)}(U_4 - U)^2)/T] \times /((1 + \exp(U_2 - U + 0.1))/0.1); \tag{17}$$

below the three-quasiparticle states excitation threshold U_3 (odd nuclei) as

$$\rho_{f(n)}(U) \cong T_{f(n)}^{-1} \exp[(U_3 + \Delta_{f(o)} - U_{f(o)} - \delta_{1f(n)})/T], \tag{18}$$

$U_f \simeq -k\Delta_f$, Δ_f being the correlation function at saddle deformations. For excitation energies above the

TABLE II. Level density parameters of U nuclei.

Nuclide	δ_{2f}	δ_{2n}	δ_{1f}	δ_{1n}
^{239}U			1.17	1
^{238}U	.85	.3		
^{237}U			1.175	1.525
^{236}U	.5	.5		

three-quasiparticle states excitation threshold U_3, but lower than the five-quasiparticle states excitation threshold U_5, the increase of the $\rho_{f(n)}(U)$ could be modelled in the same manner. Equations (17) and (18) fairly approximate the level density calculations for fixed number of quasiparticles, made for the equally spaced single-particle levels [44]. The parameter δ_{2f} for the ^{238}U fissioning nuclide helps to fit the ^{238}U(n,F) cross section steplike shape in the $E_n \gtrsim 9$ MeV. It seems we could estimate the absolute value of the ^{238}U level density at saddle deformations at excitation energies above the pairing gap, since it is correlated with the discrete levels within the pairing gap as well as the discrete levels of residual nuclide ^{237}U. The parameter δ_{1n} for the ^{237}U residual nuclide helps to reproduce the ^{238}U(n,F) cross section shape just above the second-chance fission reaction threshold, but it is not a crucial parameter, since quite a number of discrete levels of ^{237}U is available. The level density parameters $\delta_{2f(n)}$ and $\delta_{1f(n)}$ are given in Table II.

The level densities $\rho_f(U)$ of ^{238}U at the inner saddle deformations and $\rho_n(U)$ of ^{237}U at ground state deformations are shown in Figs. 2 and 3, respectively. The solid lines demonstrate the influence of few-quasiparticle excitations on the total level density $\rho_{f(n)}(U)$, as compared with the constant temperature model approximation of Eq. (16). Arrows on the excitation energy axes show the excitation thresholds U_m of few-quasiparticle states.

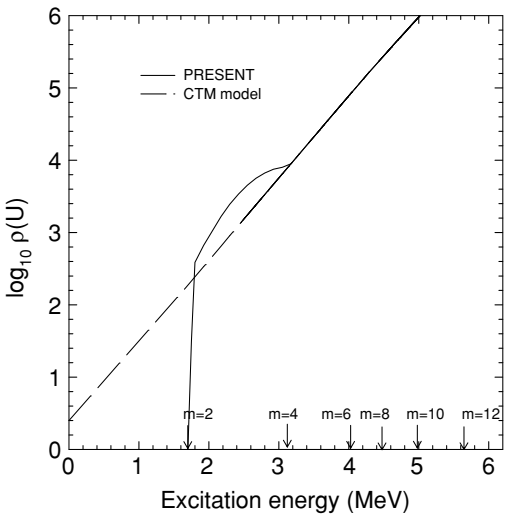

FIG. 2. Level density of ^{238}U at inner saddle deformations. Arrows on the excitation energy axis correspond to the excitation thresholds of $m = 2, 4, 6\ldots$, quasiparticle states. The solid curve is calculated using Eq. (17), the dashed curve is calculated using Eq. (16).

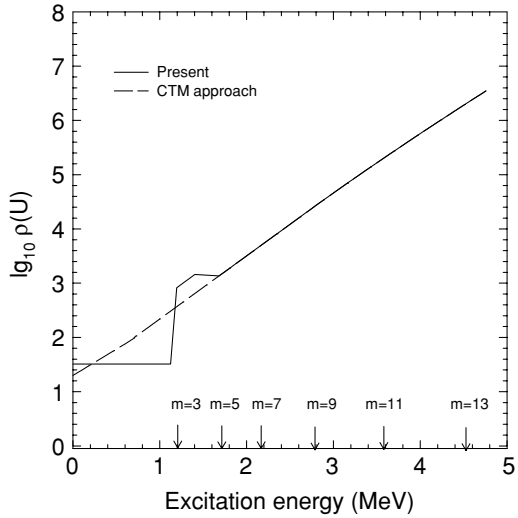

FIG. 3. Level density of ^{237}Uh at ground state deformations. Arrows on the excitation energy axis correspond to the excitation thresholds of $m = 1, 3, 5\ldots$, quasiparticle states. The solid curve is calculated using Eq. (18), the dashed curve is calculated using Eq. (16).

The main parameters of the level density model for the equilibrium, inner, and outer saddle deformations are as follows: shell correction δW, pairing correlation functions Δ_o, and Δ_f, at equilibrium and saddle point deformations. At equilibrium deformations $\Delta = 12/\sqrt{A}$, while quadrupole deformation ε and momentum of inertia at zero temperature $F_o/\hbar^2$ are given in Table III. For the ground state deformations the shell corrections were calculated as $\delta W = M^{\exp} - M^{MS}$, where M^{MS} denotes the liquid drop mass (LDM), calculated with Myers-Swiatecki parameters [49], and $M^{\exp}$ is the experimental nuclear mass. Shell correction values at inner and outer saddle deformations $\delta W_f^{A(B)}$ are adopted following the review by Bjornholm and Lynn [50].

III. FISSION DATA ANALYSIS

Neutron-induced fission cross section data [51,52] for the ^{238}U target along with the calculated $\sigma_{nF}(E_n)$ fission cross section and contributions of (n, xnf) reactions to the observed ^{238}U(n,F) fission cross section are shown on Fig. 1. Above emissive fission threshold the fission probability of

TABLE III. Level density parameters of the fissioning nucleus and the residual nuclei.

Parameter	Inner saddle	Outer saddle	Neutron channel
δW, MeV	1.5, $A \leqslant 236$	0.6	$M^{\exp} - M^{\mathrm{MS}}$
	2.6, $A > 236$	0.6	
Δ, MeV	$\Delta_o + \delta^{\mathrm{a}}$	$\Delta_o + \delta^{\mathrm{a}}$	Δ_o
ε	0.6	0.8	0.24
$F_0/\hbar^2$, MeV^{-1}	100	200	73

[a] $\delta = \Delta_f - \Delta$ value is defined by fitting the fission cross section in the plateau region.

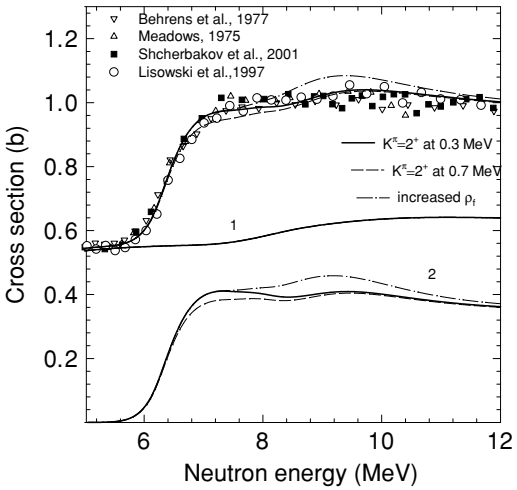

FIG. 4. ^{238}U(n,F) cross section. The solid line (present) shows a fit to the observed fission cross section, $\delta_{2f} = 0.85$ MeV; the dot-dashed line shows the sensitivity of the calculated fission cross section to the increased two-quasiparticle state density of ^{238}U at saddle deformations for $\delta_{2f} = 0.65$ MeV; dashed and solid curves show the sensitivity of the calculated fission cross section to the lowering of anomalous γ-band $K^{\pi} = 2^{+}$ of ^{238}U at outer saddle deformations due to axial asymmetric deformations. Labels "1" and "2" denote first- and second-chance fission cross sections.

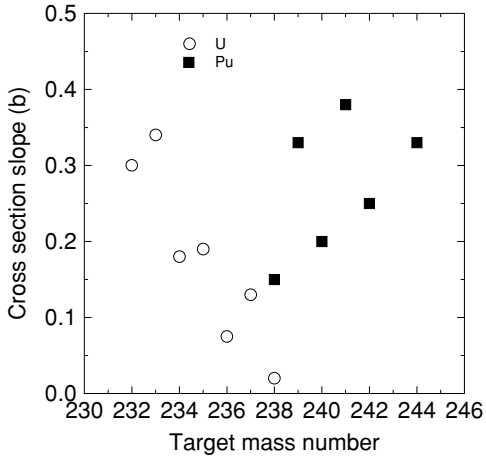

FIG. 5. Isotopic dependence of the first chance fission cross section slope $\Delta\sigma_{nf}$ for U and Pu nuclei.

^{238}U, fissioning in the ^{238}U(n, nf) reaction, could be estimated fitting the ^{238}U(n,F), ^{238}U$(n, 2n)$, and ^{238}U$(n, 3n)$ data. Just above the (n, nf) reaction threshold of $E_n \sim 6$ MeV the calculated curve fit to the measured data up to $E_n \sim 9$ MeV is affected by lowering the positions of positive parity band $K^{\pi} = 2^{+}_{1}$ at the inner (higher) barrier. The slight change of the shape of the ^{238}U(n,F) cross section above $E_n \sim 9$ MeV, could be correlated with the excitation of the two-quasiparticle states of the ^{238}U fissioning nuclide. The incident neutron energy $E_2 \sim U_2 + E_{fA(B)} + \varepsilon_1$, here ε_1 is the energy of the first prefission neutron, $E_{fA(B)}$—height of the $A(B)$ fission barrier of ^{238}U, corresponds to the excitation of the two-quasiparticle states in the fissioning ^{238}U nuclide at inner (higher) fission saddle. There is a slight systematic difference between different data sets by Lisowski *et al.* [51], Shcherbakov *et al.* [52], Behrens *et al.* [53], and Meadows [54], but a small steplike structure is evident in measured data sets around $E_n \sim 9$ MeV. Variation of the two-quasiparticle state density of ^{238}U fissioning nuclide (see Figs. 1 and 4) demonstrates quite unambiguously that the small steplike structure at $E_n \gtrsim 9$ MeV evident mostly in high-resolution data by Lisowski *et al.* [51] could be correlated with the excitation of these states at the higher (outer) saddle deformations. There are a number of measurements of ^{238}U$(n, 2n)$ reaction cross sections, which allow us to fix the ^{238}U$(n, 2n)$ cross section rather reliably (see Ref. [23] and references therein). The latest ^{238}U$(n, 2n)$ reaction cross section data are reproduced consistently with the ^{238}U(n,F) cross section (see Ref. [13]). The key parameter in definition of the ^{238}U$(n, 2n)$ reaction cross section is the preequilibrium contribution in the calculated first neutron spectrum.

Fission cross sections of $^{232-238}$U target nuclides for incident neutron energies have a number of peculiarities, which could be reproduced with the present approach. The slope of the fission cross section $\Delta\sigma_{nf}$ in the first plateau region, i.e., the difference of the cross section values at $E_n \sim 2$ MeV (the highest value in the first "plateau" region) and in the vicinity of (n, nf) reaction threshold (the lowest value in the first "plateau" region) decreases with increase of the number of neutrons in the target nucleus, in other words, the cross section shape of N-odd target nuclides ^{233}U(n, f), ^{235}U(n, f), and ^{237}U(n, f) becomes more and more flat. This peculiarity depends on the fission barriers and the ratio of the level densities of fissioning and residual nuclides. We model the slope of the fission cross section $\Delta\sigma_{nf}$ varying $\delta = \Delta_f - \Delta_o$ value, since Δ_f and Δ_o influence the main level density parameters a_f and a_n of fissioning and residual nuclides. Figure 5 shows the $\Delta\sigma_{nf}$ values for $^{232-238}$U target nuclides, it seems the slope of the predicted ^{237}U(n, f) cross section (see Figs. 6, 7, and 8) is quite compatible with that simple systematics.

Steplike structures in case of N-odd U fissile targets for $E_n \lesssim 2$ MeV could be correlated with few-quasiparticle structures level densities of even fissioning nuclei and odd residual nuclides [55]. The two-quasiparticle states of the even ^{238}U fissioning nuclide, lying below the four-quasiparticle states excitation threshold define the shape of the fission cross section below an incident neutron energy of $E_n \leqslant U_4 + E_{fA(B)} + \varepsilon_1$. Three-quasiparticle states in the even-odd residual nuclide ^{237}U could be excited after emission of two neutrons from the ^{239}U composite nuclide, the second neutron emission competes with the ^{238}U(n, nf) reaction at incident neutron energies $E_n \gtrsim B_n(^{238}\mathrm{U}) + \varepsilon_1 + \varepsilon_2 + U_3$, U_3 being the excitation threshold of the three-quasiparticle states in the even-odd residual nuclide ^{237}U, ε_2 is the energy of the second prefission neutron. At lower energies both ^{238}U(n,F) fission and ^{238}U$(n, 2n)$ cross section shapes are controlled by the one-quasiparticle state density of the even-odd residual nuclide ^{237}U.

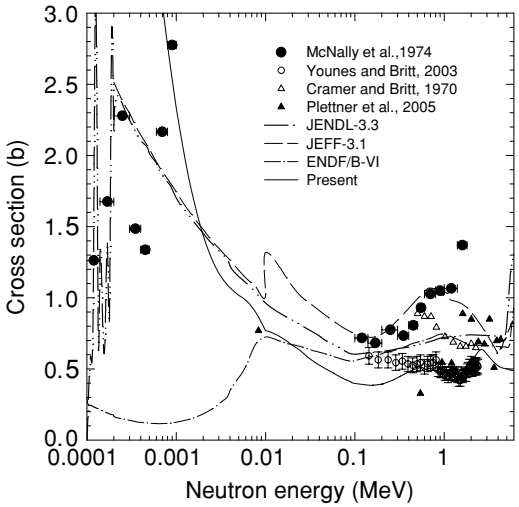

FIG. 6. ^{237}U(n, f) cross section. The solid line shows the calculated fission cross section, the dot-dashed line shows the sensitivity to the increased two-quasiparticle state density of ^{238}U at saddle deformations, $\delta_{2f} = 0.6$ MeV; dashed and solid curves show the sensitivity of the calculated fission cross section to lowering of anomalous γ-band $K^\pi = 2^+$ of ^{238}U at outer saddle deformations due to axial asymmetric deformations.

The adopted level density description of fissioning and residual nuclei allows to describe the shape of the measured fission cross section data of ^{238}U (see Figs. 1 and 4). Figures 6, 7, and 8 compare the calculated fission cross sections of the ^{237}U(n, f) reaction with the data by McNally *et al.* [1] and simulated fission cross section data obtained by Cramer and Britt [3], Younes and Britt [9], and Plettner *et al.* [11]. Previously surrogate neutron-induced fission data were obtained by Cramer and Britt [3] as $\sigma_f = \sigma_a \times P_f^{\rm exp}$, $P_f^{\rm exp}$ being

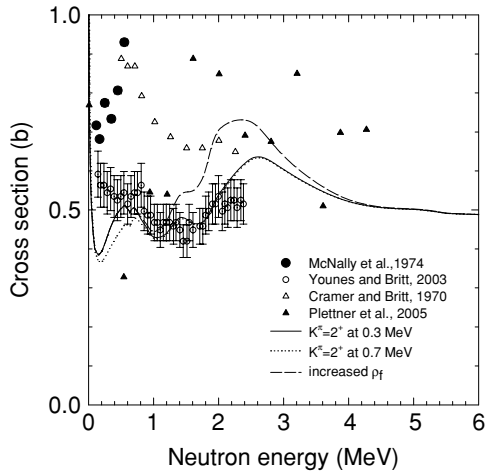

FIG. 7. ^{237}U(n, f) cross section. The solid line shows the calculated fission cross section, the dot-dashed line shows the sensitivity to the increased two-quasiparticle state density of ^{238}U at saddle deformations, $\delta_{2f} = 0.65$ MeV; dashed and solid curves show the sensitivity of the calculated fission cross section to lowering of anomalous γ-band $K^\pi = 2^+$ of ^{238}U at outer saddle deformations due to axial asymmetric deformations.

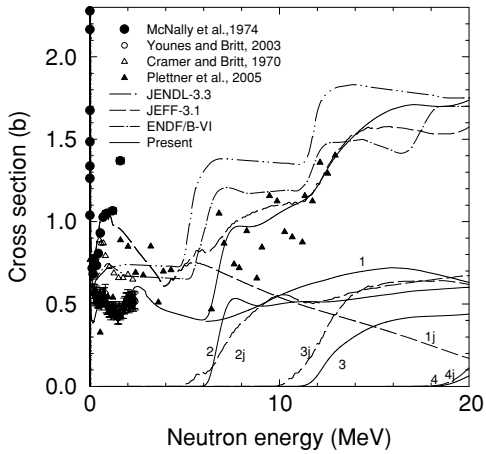

FIG. 8. ^{237}U(n, f) cross section. The solid line shows present calculated fission cross section. Labels "1," "2," "3," "4-" denote first-, second-, third-, and fourth-chance fission cross sections. Labels "1j," "2j," "3j," and "4j" denote first-, second-, third-, and fourth-chance fission cross sections of JEFF-3.1 [8] evaluation.

the fission probability, measured in the transfer reaction, the neutron absorption cross section $\sigma_a = 3.1$ barn was assumed independent on the incident neutron energy.

Since the outer barrier height E_{fB} is lower than the height of the inner barrier E_{fA}, the calculated cross section is almost insensitive to the lowering of the octupole negative parity band $K^\pi = 0_1^-$. That sensitivity was observed in case of ^{232}Th(*n*,F) reaction above the ^{232}Th(n, nf) reaction threshold [14]. On the other hand, the sensitivity to the position of the anomalous γ-band $K^\pi = 2^+$ (see Table I) is observed (see Figs. 4 and 7). Below $E_n \sim 10$ keV the major contribution comes from the *s*-wave neutrons and, consequently, from the positive parity collective bands. Figure 7 shows the discrepancy of the calculated curve and simulated data by Younes and Britt [9] when positive parity anomalous rotational band $K^\pi = 2_1^+$ both at inner (higher) saddle is at about the same excitations as at the ground state deformation. Lowering the positions of $K^\pi = 2_1^+$ band head, according to the triaxial asymmetry at inner saddle deformation, allows us to improve the description of the ^{237}U(n, f) surrogate fission data by Younes and Britt [9] at $E_n \gtrsim 0.4$ MeV (see Fig. 7), where *d*-wave neutrons start contributing. In the incident neutron energy range of 10 keV–1 MeV *p*-wave neutrons, which excite compound states with negative parity, strongly contribute to the fission cross section. However, unlike the situation observed in case of ^{231}Th(n, f) reaction [14], the calculated ^{237}U(n, f) reaction cross section is virtually insensitive to the position of $K^\pi = 0_1^-$, 1_1^-,2_1^- bands, since the outer barrier is much lower than the inner one.

The steplike structure in ^{235}U(n, f) reaction cross section at $E_n \gtrsim 0.8$ MeV [56] was shown to be a consequence of threshold excitation of two-quasiparticle states in fissioning ^{236}U nuclide and three-quasiparticle configurations in residual even-even nuclide ^{235}U [56]. However the steplike structure in the case of the ^{233}U(n, f) reaction, which could be correlated with the threshold excitation of two-quasiparticle states in fissioning ^{234}U nuclide and three-quasiparticle configurations

in residual even-odd nuclide ^{233}U, is observed at lower energies, i.e., ∼0.3 MeV [17]. In the case of ^{237}U(n, f) a similar steplike structure should be observed at still higher incident neutron energies $E_n \sim 1.2$ MeV. Figure 7 shows the sensitivity of the calculated fission cross section to the variation of the total level densities at saddle deformations $\rho_f(U)$ ($\delta_{2f} = 0.65$ MeV) (see Table II).

Above emissive fission threshold the calculated fission cross section of ^{237}U(n,F) is compared with the surrogate fission data by Plettner *et al.* [11] now available up to $E_n \sim 14$ MeV in Fig. 8. Plettner *et al.* [11] measured the ratio of fission probabilities of ^{238}U and ^{236}U nuclides for the deuteron-induced fission events, i.e., the ratio of $P_f(^{238}\mathrm{U}(d, d'f))/P_f(^{236}\mathrm{U}(d, d'f))$. Ratio data by Plettner *et al.* [11] were scanned from the figure, published in Ref. [11], precision of that procedure is quite suitable for the qualitative comparison with calculated cross sections. Under the assumption that the ratio of these fission probabilities equals the ratio of neutron-induced fission cross sections of ^{237}U and ^{235}U target nuclides, a neutron-induced fission cross section of ^{237}U target nuclide for the incident energy range of $E_n \sim 0.1$–14 MeV could be easily obtained. Figures 7 and 8 show that there is quite a scattering of the experimental data points in the first "plateau" region, as well as in the second "plateau" region, however, the present calculated cross section ^{237}U(n, f) is quite compatible with the bulk of the measured data points. There is no data point in the $E_n \sim 4$–6 MeV energy range, however, our prediction of the onset of the ^{237}U(n, nf) reaction is quite compatible with the measured data. The fission and level density parameters for the calculation of the fission probability of ^{237}U were fixed by the ^{236}U(n, f) data description [23]. Previous evaluated curves of JENDL-3.3 [4], ENDF/B-VI [5], and JEFF-3.1 [8] are shown. The calculated curve by Han [7] is not shown, however, it strongly overshoots surrogate data by Younes and Britt [9] and Plettner *et al.* [11].

There are quite a number of ^{238}U fission probability measurements in the ^{238}U$(\alpha, \alpha'\mathrm{f})$ reaction at rather high bombarding energy of α-particles, i.e., $E_\alpha = 120$ MeV [57], $E_\alpha = 172$ MeV [58], and $E_\alpha = 480$ MeV [59]. The fission probability of ^{238}U was estimated by David *et al.* [59] up to an excitation energy of ∼37 MeV. However, a drastic discrepancy of fission probabilities measured in photofission and α-particle-induced fission was observed [59], though the latter was normalized to the $P_f = 0.18$ at $U = 10$ MeV, which looks reasonable in view of recent measurement by Ref. [9]. David *et al.* [59] attributed the discrepancy to the incomplete energy transfer of inelastically scattered α-particles to the ^{238}U for excitation energies of residual nuclide ^{238}U higher than emissive fission threshold. The overall consistency of the calculated neutron-induced fission cross section of ^{237}U(n,F) with the surrogate data, obtained for $(d, d'f)$ reaction by Plettner *et al.* [11] looks quite encouraging, though rather high scattering of the measured data points is of some concern.

Neutron-induced fission cross sections of N-odd targets ^{235}U and ^{233}U for incident neutron energies E_n up to 200 MeV were measured Lisowski *et al.* [51], Shcherbakov *et al.* [52], respectively. These cross sections were described consistently up to 200 MeV in a statistical model. Fission cross section of ^{237}U with neutrons of incident neutron energies up to 200 MeV might be calculated within the same approach, assuming that the fission barrier parameters of U nuclei with $A \geqslant 236$ are fixed by ^{235}U(n,F) fission cross section description, fission barrier parameters of ^{238}U and ^{237}U are defined in this analysis. The major difference of ^{238}U and ^{237}U is the triaxiality of inner (higher) saddle, which adds an extra triaxial enhancement to the level density [see Eq. (12)]. The contributions of first- and second-chance fission reactions ^{237}U(n, f) and ^{237}U(n, nf) to the "observed" fission cross section of ^{237}U(n,F) fades away rather fast and assumptions about the damping of triaxil rotational modes would not influence much the observed fission cross section of ^{237}U(n,F).

The model for neutron-induced fission cross section calculation up to 200 MeV incident energies is described elsewhere [27,60–63]. For incident neutron energies higher than ∼20 MeV contribution of symmetric (super-long(SL)-mode [64]) fission becomes appreciable and increases rather fast, while contribution of regular asymmetric fission decreases. Symmetric and asymmetric fission reactions compete for each emissive fission ^{237}U(n, xnf) reaction. Fission barrier and level density parameter systematics are described elsewhere [61]. Damping of the axial/triaxial collective modes contribution to the level density both for inner and outer saddles and equilibrium deformations as well as triaxial damping at SL-mode outer saddle, produces symmetric/asymmetric emissive fission partitioning of ^{238}U(n,F), ^{235}U(n,F), and ^{233}U(n,F) reaction cross sections. That partitioning is based on the consistent description of observed fission cross sections and symmetric fission branching ratio for the ^{238}U(n,F) reaction. The adopted estimate of the energy-dependent asymptotic level density parameter $\tilde{a}_f$ at saddle deformations is equivalent to more fission events at lower intrinsic excitation energies, or more fission events coming from the neutron-deficient U nuclei, i.e., from higher fission chances. The damping of triaxial collective modes contributions at outer SL-mode saddle is equivalent to less symmetric fission events at higher excitation energy and more symmetric fission from neutron-deficient isotopes, as compared with the "no triaxial damping" case. The dependence of the symmetric fission branching ratio on the target nuclide fissility is interpreted as being due to the higher contribution of the lower fission chances in the case of the higher target nuclide fissilities. At the other extreme of the lower fissility target nuclei there are measured data for the ^{232}Th(n,F) reaction [52]. It turns out that the description of the observed fission cross section also could be attained only in case when more fissions come from neutron-deficient Th nuclei, i.e., from higher fission chances. The fission probability of ^{238}U at $E_n \sim 3$ MeV is rather low, only ∼2 times higher than that of ^{233}Th, however, the "observed" fission cross section of ^{237}U is similar to those of ^{235}U or ^{233}U at $E_n \gtrsim 40$ MeV. Figure 9 shows the comparison of the observed (sum of symmetric and asymmetric contributions) fission cross sections of ^{233}U(n,F), ^{235}U(n,F), and ^{237}U(n,F) for E_n up to 200 MeV. Some systematic changes of fisssion cross sections with increase of the number of neutrons is observed. Below ∼2 MeV the fission cross section becomes more "flat". The cross section slope above ∼2 MeV and up to (n, nf) reaction threshold decreases. Above the $(n, 2nf)$ reaction threshold the fission cross section increases faster. For $E_n \gtrsim 40$ MeV

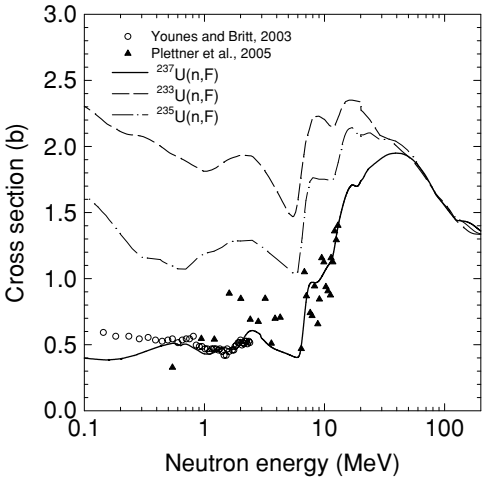

FIG. 9. ^{237}U(n, f), ^{235}U(n, f), and ^{233}U(n, f) fission cross section. The solid line shows the calculated ^{237}U(n, f) fission cross section; the dot-dashed line shows the ^{235}U(n, f) fission cross section; dashed line shows ^{233}U(n, f) fission cross section.

either ^{237}U(n,F), ^{235}U(n,F) or ^{233}U(n,F) approach the reaction cross section, in other words, the target nuclide as if lost its "personality" at sufficiently high incident neutron energies. That conclusion is compatible with the conclusion made by Ries *et al*. [65], that photofission probability of ^{238}U is almost unity for excitation energies above 40 MeV.

A. Fission barriers

It is of much interest to compare the experimental fission barriers, which are obtained by fitting measured fission cross sections, with theoretical barriers, extracted by modeling the nuclear potential energy. Our assumptions about the asymmetries and relative heights of the inner and outer fission barriers are generally supported by recent calculations of the fission barriers for U and some other actinide nuclei. Fission barriers for ^{236}U and ^{234}U were calculated with the Hartree-Fock plus BCS pairing approach by Bonneau *et al*. [66], Skyrme forces were employed. Basically, they calculated the inner barrier for the axially symmetric shape and the outer barrier for the reflection symmetric/asymmetric shapes. Reflection asymmetry at the outer saddle leads to sufficient lowering of the saddle' height [67,68]. The reflection-asymmetry near the scission point is in agreement with the mass distributions of U primary fission fragments, their estimates of the mass-asymmetric outer fission barrier for ^{236}U are quite compatible with the experimental value of fission barrier, obtained by Maslov and Hambsch [48] describing the ^{235}U(n, f) symmetric fission yield. Bonneau *et al*. [66] demonstrated that in a Hartree-Fock-Bogolyubov calculation the lowering of the outer saddle height due to the reflection-asymmetric deformations amounts to ∼5 MeV. Bonneau *et al*. [66] showed also that the triaxiality at the inner saddle of ^{236}U and ^{234}U produces only slight lowering of the barrier height.

More extensive fission barrier calculations for neutron-deficient and neutron-rich U nuclides with $230 \leqslant A \leqslant 280$ were accomplished by Mamdouh *et al*. [69,70]. These fission barrier parameters were calculated with extended Thomas-Fermi method, which is an approximation of the Hartree-Fock-Bogolyubov self-consistent mean-field (SMF) approach, plus Strutinsky integral method. Axial symmetry was assumed for the inner (lower) and outer (higher) saddles of U nuclei. The calculated outer barrier B_{out} by Mamdouh *et al*. [69] corresponds to the $E_{f\text{BAS}}$ ($AS \equiv$asymmetric fission) fission barrier for the asymmetric fission, while B_{inn} corresponds to E_{fA}.

The macroscopic-microscopic approach to the fission barrier calculations was extended recently by Moller *et al*. [71]. They defined fission barrier saddles based on a macroscopic-microscopic model, total nuclear potential energy being calculated as a function of five shape coordinates. Macroscopic part of the potential energy was calculated with a finite-range liquid-drop model (FRLDM) generalized to account for the dependencies of the macroscopic terms on the shape coordinates, i.e., elongation, necking, mass asymmetry, and deformations of the partially formed fragments. The strong point of this approach is the definition of the saddle points in a densely sampled space of five dimensions. However, it should be noted that the differences of the U outer barrier heights $E_{f\text{BAS}}(\equiv E_{fB})$ (which is higher than the inner one E_{fA}) ($232 \leqslant A \leqslant 236$) in Ref. [71] and those defined in 1995 [72], amount to ∼2 MeV, the former being rather low. As opposed to the case of ^{238}U and ^{240}U nuclides the estimates of $E_{f\text{BAS}}$ by Moller *et al*. [71] are ∼0.7 MeV higher than those of 1995 [72]. In [72] the macroscopic part of the potential energy was calculated with the finite-range droplet model (FRDM). The transition from the FRDM to the FRLDM model and a refined deformations grid strongly decreased the outer barrier height as compared with $E_{f\text{BAS}}$ of 1995 [72] fission barrier set. The $E_{f\text{BAS}}$ of 1995 [72] and Howard and Moller [28] are higher than the experimental estimates (see Fig. 10 and Table IV). Values of $E_{f\text{BAS}}$ by Moller *et al*. [71] are systematically lower than the experimental values for $A \leqslant 236$, while they almost coincide with them for ^{238}U. The compatibility of experimental and recent calculated outer fission barrier heights

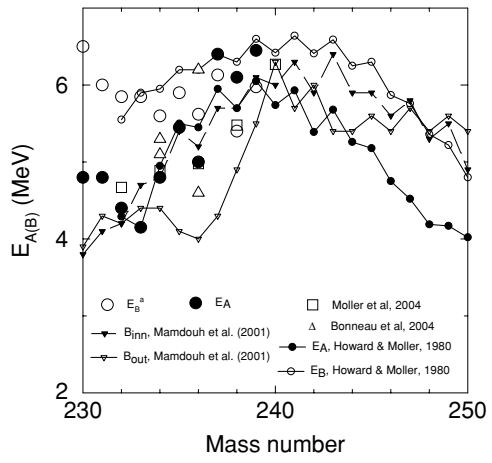

FIG. 10. Fission barriers $E_{fA(B)}$ of U nuclei.

TABLE IV. Fission barrier heights of U nuclei.

Nuclide	Inner saddle, E_{fA}				Outer saddle, $E_{f\mathrm{BAS}}$				
	Present	[28]	[69]	[66]	Present	[28]	[69]	[66]	[71]
^{239}U	6.45	6.06	6.1		5.98	6.59	5.5		
^{238}U	6.18	5.74	5.7		5.4	6.33	4.9		5.48
^{237}U	6.4	5.96	5.7		6.13	6.45	4.3		
^{236}U	5.0	5.46	5.2	6.26	5.62	6.24	4.0	4.6	4.98
^{235}U	5.45	5.53	5.4		5.9	6.24	4.1		
^{234}U	4.8	4.95	4.8	5.3	5.6	5.96	4.4	5.1	4.89
^{233}U	4.15	4.1	4.7		5.85	5.9	4.2		

by Moller *et al*. [71] has generally improved. Note that the transition from the FRDM to FRLDM is quite motivated by the shape-dependences of the macroscopic energy terms [71]. The microscopic energy models in Refs. [71] and [72] are the same, i.e., folded-Yukawa single-particle model is used in both cases. The present estimate of outer fission barrier of ^{238}U is quite compatible with calculated value by Moller *et al*. [71].

Howard and Moller [28] in extensive calculations for U nuclides with $A = 230$–276 had used a FRDM model of 1973, and a modified oscillator model for the shell/pairing correction definition. Their estimate of the $E_{fBS1(S2)}$ for $A = 230$–236 is higher that by Moller *et al*. [72] by$\sim$1 MeV, but lower by the same value for $A = 238$–240. That discussion shows that there might be some spurious isotopic dependences of microscopic/macroscopic potential energy components. Table IV compares present U ($233 \leqslant A \leqslant 239$) fission barrier heights with those calculated by Bonneau et al. [66], Mamdouh *et al*. [69,70], and Moller *et al*. [71].

IV. CONCLUSIONS

The statistical Hauser-Feshbach-Moldauer model calculation of the neutron-induced reaction cross sections for the ^{238}U target nuclide from $E_n \sim 2$ MeV up to $E_n \sim 20$ MeV allows us to extract the fission probability of ^{238}U, fissioning in the ^{238}U(n, nf) reaction, which is consistent with the ^{238}U(n,F), ^{238}U$(n, 2n)$, and ^{238}U$(n, 3n)$ data. It is quite compatible with the neutron-induced fission data for the ^{237}U target nuclide, obtained recently by Younes and Britt [9] using surrogate ^{234}U(t, pf) fission probability data. The steplike irregularity in ^{238}U(n,F) fission cross section at $E_n \gtrsim 9$ MeV is interpreted as being due to the excitation of two-quasiparticle states in the fissioning ^{238}U nuclide at saddle deformations. A similar irregularity was observed in case of the ^{232}Th(n,F) and ^{230}Th(n,F) fission cross sections [14]. The ^{238}U(n, nf) reaction contribution to the observed ^{238}U(n,F) cross section up to $E_n \sim 9$ MeV is defined by the collective levels of the ^{238}U fissioning nuclide, lying within the pairing gap. The lowering of the anomalous γ-band $K^\pi = 2^+$ due to the axial asymmetry at the inner saddle deformations seems to be important for the fission data description. It is shown to be important for the description of the ^{238}U(n,F) data in the vicinity of the ^{238}U(n, nf) emissive fission threshold and surrogate ^{234}U(t, pf) fission probability data by Younes and Britt [9]. The influence of the prefission (n, xnf) neutrons on the prompt fission neutron spectra (PFNS) for the ^{238}U(n,F) reaction on the average energy of PFNS $\langle E \rangle$ as demonstrated in Refs. [12,13], is compatible with predicted emissive fission contribution of ^{238}U(n, nf) reaction to the observed fission cross section of ^{238}U(n,F). The calculated dip in the average energy of the PFNS $\langle E \rangle$ around the ^{238}U(n, nf) reaction threshold is supported by recent measurement of prompt fission neutron spectra of ^{238}U(n,F) at $E_n \sim 6$ MeV and $E_n \sim 7$ MeV [73] and by Ethvignot *et al*. [74] at $E_n \sim 2$–200 MeV. The predicted ^{237}U(n,F) fission cross section above emissive fission threshold is generally consistent with recent surrogate data on ^{238}U$(d, d'nf)$ by Plettner *et al*. [11]. That might be additional evidence in support of developing the surrogate techniques for the estimation of fission cross sections of short-lived nuclei. The predicted ^{237}U(n,F) fission cross section up to $E_n \sim 200$ MeV is compatible with the general trend of N-odd U target fission cross sections, i.e., ^{233}U(n,F) and ^{235}U(n,F). Fission barrier parameters of U nuclei with $A \leqslant 239$, which allow us to reproduce neutron-induced fission cross sections of relevant target nuclides up to $E_n \sim$ 20 MeV, are in reasonable consistency with the theoretical fission barriers. It seems, nonetheless, that more refined investigations regarding the isotopic dependence of U inner and outer fission barriers are needed.

[1] J. H. McNally, J. W. Barnes, B. J. Dropesky *et al*., Phys. Rev. C **9**, 717 (1974).
[2] J. P. Lestone and A. Gavron, Nucl. Sci. Eng. **116**, 213 (1994).
[3] J. D. Cramer and H. C. Britt, Nucl. Sci. Eng. **41**, 177 (1970).
[4] K. Shibata, T. Kawano, T. Nakagawa *et al*., J. Nucl. Sci. Technol. **39**, 1125 (2002).
[5] R. W. Roussin, P. G. Young, and R. McKnight, in *Proceedings of the International Conference on Nuclear Data for Science and Technology, Gatlinburg*, USA, 9–13 May, 1994, edited by J. K. Dickens, ANS, 1994, p. 692.
[6] P. G. Young, M. B. Chadwick, R. E. MacFarlane *et al*., in *Proceedings of the International Conference on Nuclear Data*

for Science and Technology, Santa Fe, USA, 26 September–1 October, 2004, edited by R. C. Haight, M. B. Chadwick, T. Kawano, and P. Talou (AIP, New York, 2005), p. 290.
[7] Y. Han, Nucl. Sci. Eng. **150**, 170 (2005).
[8] JEFF-3.1 (CD-ROM), published 2 June 2005, NEA #06071 (available also via http://www.nea.fr/html/dbdata/JEFF/index.html).
[9] W. Younes and H. C. Britt, Phys. Rev. C **68**, 034610 (2003).
[10] W. Younes and H. C. Britt, Phys. Rev. C **67**, 024610 (2003).
[11] C. Plettner, H. Ai, and C. W. Beausang *et al*., Phys. Rev. C **71**, 051602(R) (2005).
[12] V. M. Maslov, Yu. V. Porodzinskij, M. Baba, A. Hasegawa, N. V. Kornilov, A. B. Kagalenko, and N. A. Tetereva, Phys. Rev. C **69**, 034607 (2004).
[13] V. M. Maslov, Yu. V. Porodzinskij, M. Baba, A. Hasegawa, N. V. Kornilov, A. B. Kagalenko, and N. A. Tetereva, Eur. Phys. J. A **18**, 93 (2003).
[14] V. M. Maslov, Nucl. Phys. **A743**, 236 (2004).
[15] V. M. Maslov, N. V. Kornilov, A. B. Kagalenko, and N. A. Tetereva, Nucl. Phys. **A760**, 274 (2005).
[16] V. M. Maslov, Yu. V. Porodzinskij, M. Baba, A. Hasegawa, N. V. Kornilov, A. B. Kagalenko, and N. A. Tetereva, INDC(BLR)-17 (2003), IAEA, Vienna, Austria (available also via http://www-nds.iaea.org/reports/indc-blr-017.pdf).
[17] V. M. Maslov, Yu. V. Porodzinskij, M. Baba, A. Hasegawa, N. V. Kornilov, A. B. Kagalenko, and N. A. Tetereva, INDC(BLR)-18 (2003), IAEA, Vienna, Austria (available also via http://www-nds.iaea.org/reports/indc-blr-018.pdf).
[18] V. M. Maslov, Nuclear Reaction Data and Nuclear Reactors, Trieste, Italy, 2000, ICTP, 2001, pp. 231–268.
[19] Handbook for Calculations of Nuclear Reaction Data: Reference input parameter library, IAEA-TECDOC-1034, 1998, Vienna, p. 81.
[20] A. V. Ignatjuk and V. M. Maslov, *Proceedings of the International Symposium on Nuclear Data Evaluation Methodology*, Brookhaven, USA, 12–16 October 1992 (World Scientific, New York, 1993), p. 440.
[21] V. M. Maslov and Y. Kikuchi, JAERI-Research 96-030, 1996.
[22] M. Uhl and B. Strohmaier, IRK-76/01, IRK, Vienna (1976).
[23] V. M. Maslov, Yu. V. Porodzinskij, M. Baba, A. Hasegawa, N. V. Kornilov, A. B. Kagalenko, and N. A. Tetereva, INDC(BLR)-014, Vienna, 2003.
[24] P. A. Moldauer, Phys. Rev. C **11**, 426 (1975).
[25] V. M. Maslov, Yu. V. Porodzinskij, M. Baba, and A. Hasegawa, Nucl. Sci. Eng. **143**, 177 (2003).
[26] J. W. Tepel, H. M. Hoffman, and H. A. Weidenmuller, Phys. Lett. **B49**, 1 (1974).
[27] V. M. Maslov, Yu. V. Porodzinskij, M. Baba, A. Hasegawa, and N. A. Tetereva, Nucl. Phys. **A736**, 77 (2004).
[28] W. M. Howard and P. Möller, At. Data Nucl. Data Tables **25**, 219 (1980).
[29] V. M. Maslov and Y. Kikuchi, Nucl. Sci. Eng. **124**, 492 (1996).
[30] M. Csatlos, A. Krasznahorkay, P. G. Thirolf *et al*., Phys. Lett. **B615**, 175 (2005).
[31] V. M. Strutinsky, Nucl. Phys. **A95**, 420 (1967).
[32] A. Gavron, H. C. Britt, P. D. Goldstone, J. B. Wilhelmy, and S. E. Larsson, Phys. Rev. Lett. **38**, 1457 (1977).
[33] M. Shmorak, Nucl. Data Sheets **36**, 367 (1982).
[34] V. M. Maslov, Yu. V. Porodzinskij, M. Baba, A. Hasegawa, N. V. Kornilov, A. B. Kagalenko, and N. A. Tetereva, INDC (BLR)-014, Vienna, 2003.
[35] V. M. Maslov, Yu. V. Porodzinskij, M. Baba, and A. Hasegawa, Izv. Ros. Akad. Nauk. Ser. Fiz. **67**, 1597 (2003).
[36] V. M. Maslov, Yu. V. Porodzinskij, M. Baba, and A. Hasegawa, *Proceedings of the Eleventh International Symposium on Capture Gamma-Ray Spectroscopy and Related Topics*, 2–6 September, 2002, Prague, p. 753–756.
[37] V. M. Maslov, Yu. V. Porodzinskij, M. Baba, A. Hasegawa, and N. A. Tetereva, Nucl. Phys. A, accepted for publication (2005).
[38] V. M. Maslov, Yu. V. Porodzinskij, M. Baba, A. Hasegawa, N. V. Kornilov, and A. B. Kagalenko, *Proceedings of the International Conference on Nuclear Data for Science and Technology*, 7–12 October, 2001, Tsukuba, Japan, 2002 p. 148.
[39] A. J. M. Plompen, C. Goddio, V. M. Maslov, Yu. V. Porodzinskij, *Proceedings of the VIII International Seminar on Interaction of Neutrons with Nuclei, Dubna, Russia*, 17–20 May, 2000 (2000), p. 153.
[40] J. E. Lynn and A. C. Hayes, Phys. Rev. C **67**, 014607 (2003).
[41] A. V. Ignatjuk, K. K. Istekov, and G. N. Smirenkin, Sov. J. Nucl. Phys. **29**, 450 (1979).
[42] V. M. Maslov, Phys. At. Nucl. **63**, 161 (2000).
[43] V. M. Maslov and Yu. V. Porodzinskij, JAERI-Research 98-038, Japan, 1998.
[44] A. V. Ignatyuk, Statistical Properties of Excited Atomic Nuclei, Energoatomizdat, Moscow, 1983 (in Russian); INDC-223(L), IAEA, Vienna, 1985.
[45] P. Demetriou and S. Goriely, Nucl. Phys. **A695**, 95 (2001).
[46] C. Fu, Nucl. Sci. Eng. **86**, 344 (1984).
[47] V. M. Maslov, Z. Phys. A: Hadrons & Nuclei, **347**, 211 (1994).
[48] V. M. Maslov and F.-J. Hambsch, Nucl. Phys. **A705**, 352 (2002).
[49] W. O. Myers and W. J. Swiatecky, Ark. Fys. **36**, 243 (1967).
[50] S. Bjornholm and J. E. Lynn, Rev. Mod. Phys. **52**, 725 (1980).
[51] P. W. Lisowski, A. Gavron, W. E. Parker *et al*. *Proceedings of the Specialists' Meeting on Neutron Cross Section Standards for the Energy Region Above 20 MeV*, Uppsala, Sweden, 21–23 May, 1991 (OECD, Paris, 1991), p. 177.
[52] O. A. Shcherbakov *et al*., *Proceedings of the International Conference on Nuclear Data for Science and Technology*, Tsukuba, Japan, 7–12 October, 2001 (2002), p. 230.
[53] J. W. Behrens and G. W. Carlson, Nucl. Sci. Eng. **63**, 250 (1977).
[54] J. W. Meadows, Nucl. Sci. Eng. **58**, 255 (1975).
[55] V. M. Maslov, Fission Level Density and Barrier Parameters for Actinide Neutron-Induced Cross Section Calculations, INDC(BLR)-013, (1998), IAEA, Vienna, Austria (available also via http://www-nds.iaea.org/reports/indc-blr-013.pdf).
[56] A. V. Ignatyuk and V. M. Maslov, Phys. At. Nucl. **54**, 392 (1991).
[57] R. de Leo, M. N. Harakeh, S. Micheletti *et al*., Nucl. Phys. **A373**, 509 (1982).
[58] H. P. Morsch, M. Rogge, P. Decowski *et al*., Phys. Lett. **B119**, 315 (1982).
[59] P. David, J. Hartfield, H. Janszen *et al*., Z. Phys. A: At. Nucl. **326**, 367 (1987).
[60] V. M. Maslov, Nucl. Phys. **A717** 3 (2003).
[61] V. M. Maslov, Phys. Lett. **B581**, 55 (2004).
[62] V. M. Maslov, Eur. Phys. J. A **21**, 281 (2004).
[63] V. M. Maslov, Nucl. Phys. **A757**, 390 (2005).
[64] U. Brosa, S. Grossmann, and A. Müller, Phys. Rep. **197**, 167 (1990).
[65] H. Ries, U. Kneissl, G. Mank *et al*., Phys. Lett. **B139**, 254 (1984).
[66] L. Bonneau, P. Quentin, and D. Samscen, Eur. Phys. J. A **21**, 391 (2004).
[67] P. Moller and S. G. Nilsson, Phys. Lett. **B31**, 283 (1970).

[68] V. V. Pashkevich, Nucl. Phys. **A169**, 275 (1971).
[69] A. Mamdouh, J. M. Pearson, M. Rayet, and F. Tondeaur, Nucl. Phys. **A644**, 337 (1998).
[70] A. Mamdouh, J. M. Pearson, M. Rayet, and F. Tondeaur, Nucl. Phys. **A679**, 337 (2001).
[71] P. Moller, A. J. Sierk, and A. Iwamoto, Phys. Rev. Lett. **92**, 072501 (2004).
[72] P. Moller, J. R. Nix, W. D. Myers, and W. J. Swiatecki, At. Data Nucl. Data Tables **59**, 185 (1995).
[73] G. N. Lovchikova, A. M. Trufanov, M. I. Svirin *et al*., Physics of Atomic Nuclei **67**, 628 (2004).
[74] T. Ethvignot, M. Devlin, R. Drosg, T. Granier, R. C. Haight, B. Morillon, R. O. Nelson, J. M. O'Donnel, and D. Rochman, Phys. Lett. **B575**, 221 (2003).